Disorder induced power-law gaps in an Insulator-Metal Mott transition

Zhenyu Wang[1], Yoshinori Okada[2], Jared O'Neal[3], Wenwen Zhou[4], Daniel Walkup[5], Chetan Dhital[6], Tom Hogan[7], Patrick Clancy[8], Young-June Kim[8], Y.F Hu[8], Luiz Santos[1], Stephen Wilson[9], Nandini Trivedi[10], Vidya Madhavan[1]

[1]UIUC, [2]OIST, [3]ANL, [4]Boston College, [5]NIST, [6]LSU, [7]UCSB, [8]University of Toronto, [9]University of California, Santa Barbara, [10]The Ohio State University

Submitted to Proceedings of the National Academy of Sciences of the United States of America

A correlated material in the vicinity of an insulator-metal transition (IMT) exhibits rich phenomenology and variety of interesting phases. A common avenue to induce IMTs in Mott insulators is doping, which inevitably leads to disorder. While disorder is well known to create electronic inhomogeneity, recent theoretical studies have indicated that it may play an unexpected and much more profound role in controlling the properties of Mott systems. Theory predicts that disorder might play a role in driving a Mott insulator across an IMT, with the emergent metallic state hosting a power law suppression of the density of states (with exponent close to 1; V-shaped gap) centered at the Fermi energy. Such V-shaped gaps have been observed in Mott systems but their origins are as yet unknown. To investigate this, we use scanning tunneling microscopy and spectroscopy to study isovalent Ru substitutions in $Sr_3(Ir_{1-x}Ru_x)_2O_7$ ($0 \le x \le 0.5$) which drives system into an antiferromagnetic, metallic state. Our experiments reveal that many core features of the IMT such as power law density of states, pinning of the Fermi energy with increasing disorder, and persistence of antiferromagnetism can be understood as universal features of a disordered Mott system near an IMT and suggest that V-shaped gaps may be an inevitable consequence of disorder in doped Mott insulators.

correlated | disorder | gap

Metal-insulator transitions are observed in a range of material systems from uncorrelated metals to correlated insulators[1-3]. One could start from a non-interacting `good' metal and turn it into an insulator by adding disorder as in an Anderson transition[4]. The single particle excitations in the resulting insulator remain gapless. One could also start with an interacting system such as a correlated insulator with a well-defined gap in the single particle density of states (DOS) as described by the Mott-Hubbard model[5] and turn it into a `bad' metal by doping. In the latter scenario, disorder is an inevitable byproduct of doping and the interplay between correlations[2,6], doping[7] and disorder pose fundamental challenges for theory and experiment. While it is well established that disorder can lead to a soft gap in the DOS of metals[8] or insulators[9, 10] with long-range coulomb interactions, it is only recently that theoretical studies have addressed the effect of disorder on the DOS of Mott systems,[11-18] with intriguing predictions of insulator-metal transitions (IMT) and a power-law (V-shaped) suppression of the density of states on the metallic side. Experimentally, disorder is well known to create an inhomogeneous potential landscape. However, whether disorder might lead to power law gaps in Mott systems, remains a key outstanding question that has not yet been experimentally addressed. This is a particularly important question since strikingly linear DOS suppressions are ubiquitously observed in doped Mott systems, e. g., various cuprate series[19-22], iridium oxide[23,24], Se doped 1T-TaS_2 (ref. 25) and Cu substituted iron pnictides[26,27] (details shown in supplementary information (SI) I), but their origins remain a mystery.

The iridium oxide compounds (iridates) provide an ideal platform to address the effect of disorder in Mott systems. The parent compounds of the layered iridate $Sr_{n+1}Ir_nO_{3n+1}$ (n=1, 2) host novel $J_{eff}=1/2$ Mott ground states, where strong spin-orbit coupling and crystal field effects split the $5d^5$ t_{2g} manifold into an occupied $J_{eff}=3/2$ and a narrow half-filled $J_{eff}=1/2$ band, which in turn amplifies correlation effects and results in a Mott-antiferromagnetic insulator[28, 29]. Electron doping these materials has been shown to result in intriguing phenomena which parallel the hole-doped cuprates[30, 31] Among the iridates, pristine $Sr_3Ir_2O_7$ (Ir327) exhibits a smaller charge gap ($\Delta E \sim 130$meV) and is ideally suited to scanning tunneling microscopy (STM) studies[32].

In this work we focus on Ru-substituted Ir327. One of the biggest problems in studying disorder effects experimentally is that doped Mott systems often host a variety of competing phases, which makes it extremely difficult to isolate the effects of disorder. Figure 1A depicts the electronic phase diagram of $Sr_3(Ir_{1-x}Ru_x)_2O_7$ which has been well established in our previous study[33]. As seen in the phase diagram, other than antiferromagnetism (AFM), there is a distinct absence of additional order parameters. In addition, in current study, we constrain ourselves to Ru concentrations far from the paramagnetic phase boundary in the region where static AFM is robust and its fluctuations play a minimal role. Furthermore, our STM data show that Ru acts as a weak scatterer and unlike most other impurities does not induce in-gap impurity states. The lack of competing phases, and the role of Ru as a weak perturbant make $Sr_3(Ir_{1-x}Ru_x)_2O_7$ an ideal system to study the effects of disorder on the DOS in Mott insulators.

Significance

Correlated electron systems often show unexpected behavior that defies theoretical explanations. One such mystery is the universal presence of V-shaped gaps with surprisingly linear energy dependence, whose origins are as yet unknown. Conventional wisdom implicates static order like charge density waves, or fluctuations of a nearby order parameter like superconductivity or antiferromagnetism. However, adding dopants to correlated systems inevitably leads to the opposite of order—i.e., electronic disorder, which begs the question: could disorder create well-defined signatures in electronic properties? By carefully choosing a material with no additional order, we show that order is not the only path to gaps, and that disorder may play a surprising role in generating universal signatures in the density of states of disordered correlated systems.

Reserved for Publication Footnotes

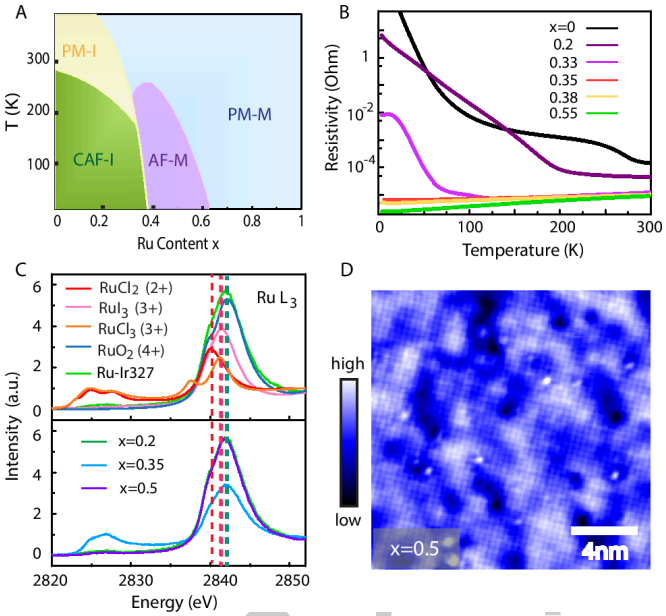

Fig. 1. Insulator-metal transition in $Sr_3(Ir_{1-x}Ru_x)_2O_7$.(A)Phase diagram of $Sr_3(Ir_{1-x}Ru_x)_2O_7$ established by bulk susceptibility, neutron scattering and transport measurements in ref. 33. CAF-I: insulating canted AF phase; PM-I: paramagnetic insulating phase; AF-M: AF ordered metallic phase; PM-M: paramagnetic metal. (B) Temperature-dependent resistivity for different Ru concentrations. IMT takes place at the critical concentration of x∼0.37. (C) Comparison of the Ru oxidation state in $Sr_3(Ir_{1-x}Ru_x)_2O_7$ with other reference samples using X-ray absorption spectroscopy. The oxidation states of Ru in $RuCl_2$, RuI_3, $RuCl_3$ and RuO_4 are 2+, 3+, 3+ and 4+ respectively. (D) Topography taken on 50% Ru-doped samples. Scanning conditions: V_b=200mV, I=50pA. V_b: sample bias with respect to the tip; I: set point current.

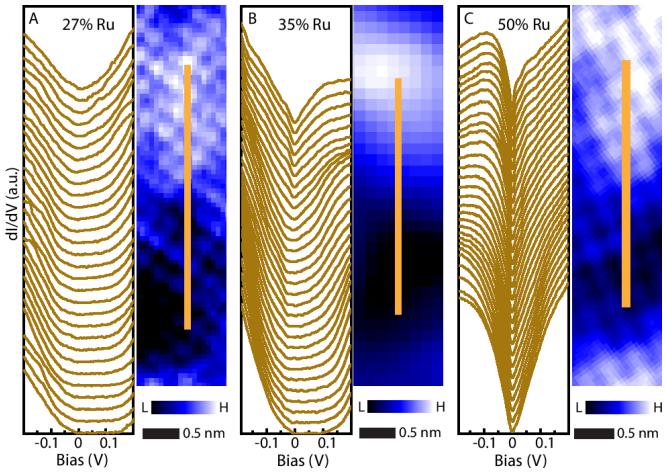

Fig. 2. *dI/dV* line cuts across IMT in $Sr_3(Ir_{1-x}Ru_x)_2O_7$. Line cuts and the associated topographic images indicating where the line cuts were obtained in: (A) 27%, (B) 35%, and (C) 50% Ru-substituted samples. The spectra in A and B show the evolution from gapped and insulating line-shape (27%), to relatively smaller gap and more metallic behavior (35%). The spectra of 50% Ru-doped sample shown in C, however, exhibit V-shaped DOS almost along the whole line. STM setup condition in all panels: V_b=-200mV, I=100pA. The spectra have been shifted vertically for clarity.

While 5% of electron doping[34] or 15% of hole doping[35] is sufficient to drive the layered iridates across Mott transition, up to 37% in-plane Ru substitution is required to collapse the parent Mott state (Fig. 1B). This then begs the question: do the Ru substituents donate itinerant charge to Ir327 thereby acting as dopants? The question of doping in a correlated system is a complex one. It has been shown that substitutional atoms which may naively be expected to dope a Mott system either by moving the Fermi energy into the bands (rigid band shift) or by creating an impurity band, actually have a much more complicated behavior[36,37]. Calculations for 3d and 4d substitutional dopants in iron pnictides suggest that in some cases, any extra charge that was supposed to have been responsible for doping, remains tightly bound to the substituent atom, which therefore effectively acts as an isovalent impurity. Similarly, we find that Ru goes into the lattice with a 4^+ valence state identical to Ir, making it an isovalent substitutional impurity i.e., an ion with the same oxidation state as Ir, with any added electrons or holes remaining localized.

The strongest evidence of this comes from our X-ray absorption spectroscopy (XAS) studies. In XAS measurements, shifts in white-line peaks (strong sharp peaks in absorption spectra) indicate a well-defined chemical shift that is proportional to the valence of the absorbing ion. As an example, Rh substitutions in Sr_2IrO_4 which should naively be isovalent, have instead been shown to have a valance of 3^+ using the L_3 edge in XAS spectra which arises from the $2p_{3/2}$ to 4d transition[35,38]. The role of Rh as a hole dopant in this system was also confirmed by the corresponding change in the valence state of Ir from 4^+ to a mixture between 4^+ and 5^+ (ref.38). A similar analysis can be carried out for our samples. Comparison of the L_3 peaks in $Sr_3(Ir_{1-x}Ru_x)_2O_7$ with reference samples are shown in Fig. 1C. The position of the L_3 peaks in Ir327 indicates that Ru is in the 4^+ state across all concentrations from x=0.2 to x=0.5. Moreover, the width of the white-line also does not change which indicates no significant change in the distribution of Ru valences in this doping range (SI II). A similar result can be observed at the Ru L_2 edge ($2p_{1/2}$ to 4d states) as well, as shown in SI II. These observations imply that Ru acts as an isolavent substituent in this system. This finding is corroborated by recent x-ray data[39,40] which additionally show that Ir retains a formal valence of 4^+ even at high Ru substitutions. Taken together with our STM measurements where the Fermi energy does not move into the valence band with increasing Ru doping, we conclude that the Ru does not significantly change the itinerant carrier concentrations at these dopings, which explains the large amount of Ru needed to make the system metallic.

Ir327 is composed of alternating IrO_6 bilayers separated by rock-salt SrO spacers. Cleavage occurs easily between two adjacent SrO layers, resulting in a charge-balanced surface. Figure 1D depicts a typical STM topograph obtained on a x=0.5 sample. The Sr atoms form a square lattice with lattice constant a=3.9Å. It is difficult to see the individual Ru atoms in this image because Ru substitutes on the Ir sites, which lie 2.0 Å below the SrO plane. However, at higher Ru concentrations we observe patches of bright regions in the topography, which as we will see later represent areas with a smaller gap magnitude caused by the Ru substitution. A comparison of the topographies for samples with different Ru doping levels can be found in SI III.

Local electronic structure can be probed by a differential conductance (dI/dV) measurement which is proportional to the local DOS. We start with the parent compound which has been discussed in detail in our earlier paper[32]. The spatially averaged dI/dV spectrum obtained on defect-free regions of the undoped sample is shown in SI IV. The DOS in an energy range from -10meV to +120meV is suppressed to zero, resulting in a hard Mott gap ∼130meV with Fermi level positioned close to the top of the lower Hubbard band. To study the effect of Ru substitution, we first examine spatially resolved dI/dV spectra collected along a line (linecut) in samples with varying Ru concentration across the IMT. At x∼27% Ru doping, transport properties indicate an insulating behavior, with neutron scattering showing robust AFM, confirming that the compound is still in the Mott phase. Figure 2A displays a linecut across dark and bright regions of the topography

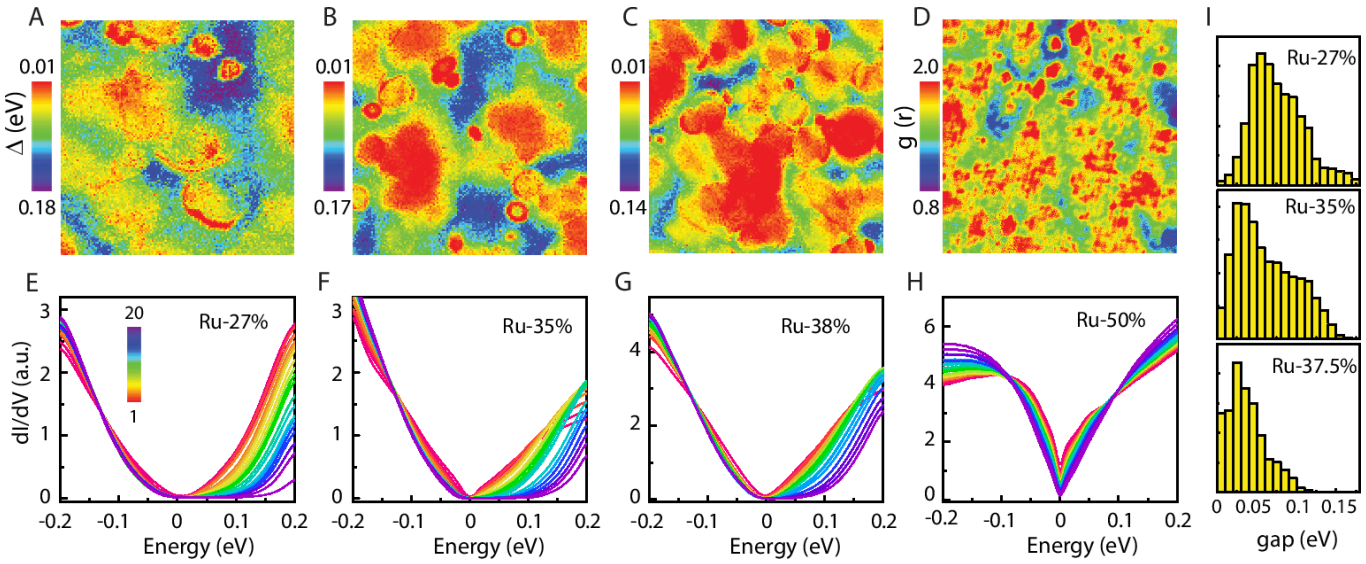

Fig. 3. Spatial evolution of *dI/dV* spectra for a wide range of Ru substitution. (A-C) Gap maps showing the spatial inhomogeneity. The metallic regions expand (red) as the Ru concentration increases, indicating the trend towards an IMT. (D) *dI/dV* conductance map at +30mV for x=0.5 Ru- substituted sample. (E-G) Averaged *dI/dV* spectra for x∼27%, x∼35% and x∼38%, respectively. To create these averages, spectra in the dI/dV maps were sorted by the gap magnitude into bins and then each bin was averaged. The spectra were split into ∼20 bins with equal population, ranging from the ones with the largest gap (blue/purple) to the ones with zero gap (red). The colors for the spectra at each doping depict the spectra in the same color regions of the gap maps at that doping. (H) Averaged spectra which are classified by the conductance value at +30mV. At this Ru concentration, all spectra are gapless. The color scale indicates the conductance value (see section VIII). (I) Histograms of the spectral gap magnitude. The average gap size shrinks as the Ru substitution increases.

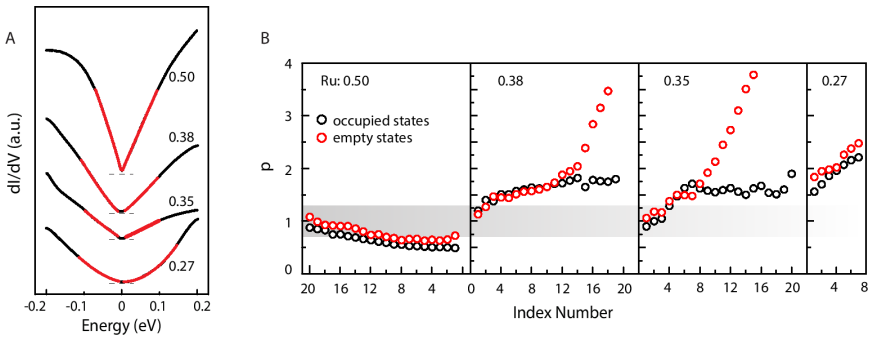

Fig. 4. Characterizing the V-shape gap. (A) Fit to the most metallic dI/dV spectra shown in Fig. 3 for x=0.27, 0.35 and 0.38 , and the most V- shaped one in Ru=0.5, with . The spectra have been shifted vertically for clarity, and the dashed lines denote the position of zero conductance for each curves. (B) Range of fitting parameter *p* for the data shown in Fig. 3E-H. The index numbers label the bins described in Fig. 3. A smaller power corresponds to a more metallic spectrum.

at this doping. The tunneling spectra show pronounced spatial variations: in the dark region, the DOS is zero for the energy range from -10 to +100 meV, yielding a gap size of ∼110 meV; This gap becomes much narrower when approaching a bright region. Although the connection between Ru substitutions and bright areas is not at first obvious, the local electronic structure shows a clear trend with increasing Ru doping. In the x∼35% sample which lies near the IMT (Fig. 2B), the insulating gap obtained in the dark areas diminishes (∼80meV), and even vanishes in the bright area, changing into a V-shaped gap. Note that the term `V-shape' is used in this paper to describe the power law (almost linear) dependence of the DOS on energy. This particular spectral shape will be discussed in further detail later. The sample with x∼50% is on the metallic side of the IMT and the linecut shown in Fig. 2C reveals that spatial inhomogeneity persists into this nominal metal. However, other than some extremely Ru-rich regions where the spectra are similar to that of $Sr_3Ru_2O_7$ (ref.41), the data now predominantly show a V-shaped gap.

While spectra in line cuts provide a glimpse into the evolving spectral features across the IMT, to obtain a more complete picture, we acquire *dI/dV* (r, V) spectra on a densely-spaced 2D grid (*dI/dV* map) for each doping (SI V). The magnitude of the charge gap is then extracted at each location in the grid (SI VI) and we plot the 2D gapmaps in Fig. 3A-C. To understand the range of spectra within each sample and to see how the spectral shapes evolve with doping, we sort the spectra for each map into bins defined by the gap magnitude, and display the averaged spectrum for each bin (Fig. 3E-H). Further details of the sorting procedure are in SI VII. The gap maps are color coded to match the spectra; i.e., red/blue/green areas of the map for a particular doping, correspond to the red/blue/green *dI/dV* spectral shapes shown for that doping.

At x∼27%, consistent with the insulating behavior of the resistivity, the sample shows gapped spectra in most areas (Fig. 3A and E) with an average gap of 72meV (as shown by the histogram in Fig. 3I). Very close to the IMT, at x∼35%, the gap histogram shifts to lower energies and the average gap is ∼40 meV. Clear V-shaped gap features can now be seen that cover about 20% of the sample (red areas). We associate these V-shaped areas with metallic regions. Eventually at the IMT at x∼37.5% (Fig. 3C and G), the regions showing V-shaped spectra become predominant. The metallic regions have grown in spatial extent and now mutually connect (red and yellow in the gapmap), in agreement with a quantum percolation driven IMT transition proposed in transport studies[42]. Finally, we turn to the metallic x∼50% compound. To obtain a visual sense of the variation of the spectra in this gapless 50% sample, a *dI/dV* conductance map at 30meV is plotted in Fig. 3D and the associated spectra are shown

in Fig. 3H. We see that the sample on the metallic side continues to remain inhomogeneous. The metallicity is represented by the pervasive V-shape of the spectra, and the inhomogeneity is represented by the variation in spectral lineshapes. We note here that while the spectral shapes differ with location and doping, the Fermi level is always pinned close to the top of lower Hubbard band.

Discussion and Summary

The question we seek to address is: how do we understand striking V-shaped gap observed in $Sr_3(Ir_{1-x}Ru_x)_2O_7$? Similar gaps have been seen in other Mott systems and are often attributed to the emergence or fluctuations of an order parameter. This is however an unlikely explanation for the V-shaped gap seen in our data. Unlike hole doped cuprates[19, 21, 22] and the electron doped single layer iridates[23], and consistent with the phase diagram established in earlier studies (Fig. 1A), no sign of additional charge order is observed either in real or momentum space in this system (SI IX). Combined with the absence of superconductivity in this phase diagram, we rule out new order parameters or preformed pairs as the cause of this gap. Another possibility suggested by calculations is that the soft gap arises from AFM fluctuations. However, in our case, it is clear from neutron scattering data[33] that static AFM persists deep into the metallic phase where the V-shape gap is pervasive. In fact, the phase transition into the paramagnetic state occurs at much higher percentages of Ru (>65%). As shown in SI X, near IMT, the coherence length of AFM order is larger than 200 Å in real space and one order of magnitude larger than that of V-shaped DOS region. Since we observe a pervasive V-shaped gap in the metallic sample with robust long-range AFM, it is unlikely that AFM fluctuations are the cause of this gap.

To explain this phenomenology, we turn to the disordered Hubbard model, which incorporates disorder as a random site dependent potential variation. While this may be a simplistic model for our system, it is fruitful to compare the theoretical results with our experimental data to look for universal signatures of a disordered Mott system. The disordered Hubbard model has been numerically studied in the last decade both by Hartree-Fock[11,14] as well as quantum Monte Carlo techniques[13] (SI XI). We reproduced the Hartree-Fock calculations with a more realistic disorder potential and the results show remarkable similarities with our data (SI XII). First, with increasing disorder fraction, the Mott gap gradually closes; second, the Fermi level is pinned at the top of lower Hubbard band and the Mott gap fills up by states being pulled in from the upper Hubbard band; and third, after the IMT, the calculated spectra show a characteristic V-shape similar to our data. Interestingly, the simulations also show a pronounced spatial inhomogeneity of DOS, where Mott-gapped insulating regions coexist with -V-shape gapped metallic regions. These multiple observations taken together suggest that the V-shaped gap may be attributed to the effects of disorder on the electronic structure of a Mott insulator.

To further establish the relationship between the observed gap and a disordered Mott system, we look for a universal scaling relationship of the density of states with energy $D(\epsilon)$. We find that most of the numerical calculations using the Hubbard model predict a power-law dependence[12-14,43,44] for $D(\epsilon)$. We track the power-law exponent in the experimental data across the IMT by fitting the tunneling spectra shown in Fig. 3E-H with a power-law function $D(\epsilon) \sim |\epsilon - \epsilon_F|^{\mathcal{P}}$ in energy range about [-50meV, 50meV]. The fitting parameter $\mathcal{P}$ for each indexed spectrum is plotted in Fig. 4B. Since each sample shows a range of spectral shapes, the value of the exponent correspondingly varies. However, we see a clear trend across the IMT. If we consider the most metallic spectra for each doping for example, we find that the exponent □ changes from a value around 2 (U-shaped) in the 27% samples to about 1 in the inhomogeneous metallic samples, for both the occupied and empty states, confirming the that the suppression in the DOS is quite linear at low energies (Fig. 4A and B). The fitting procedure applied on the individual spectra of Fig.2 gives a similar trend, as shown in SI XIII. The change in exponent from 2 to 1 is a non-trivial occurrence in both theory and experiment and a simple band closing picture due to either carrier doping or reduced spin-orbit coupling, cannot capture the linear behavior of the DOS. Interestingly, a heuristic statistical model can be constructed to explain how a linear DOS might arise in a standard Anderson-Hubbard model in the highly disordered regime (SI XIV). We note that while the heuristic relies on large values of on-site repulsive potential U and disorder strength V, the parameters used in the Hartree-Fock calculations in contrast are completely within the expectations for the iridates. While simplistic, the heuristic serves to motivate the general observations of the V-shaped gaps in Mott systems.

On comparing our findings with other Mott systems (SI I), we observe many common features including IMTs which proceed through spatial inhomogeneity and V-shaped gap formation. In $SrRu_{1-x}Ti_xO_3$, for example, which is another candidate to reveal the nature of disorder in strong correlated systems, a nearly linear energy dependence of DOS has been found[45]. Gaps with similar lineshapes have also been reported in many doped oxides including other iridates[23, 24, 35], underdoped cuprates[19-22, 46, 47], and manganites[48], making it is essential to consider disorder effects in these systems. While the complex phenomenology of the cuprates and iridates cannot all be captured by disorder effects, disorder may be implicated in the overall linear suppression of density of states near the Fermi energy in these systems.

In correlated metals, it has been shown both theoretically and experimentally that disorder can cause localization and decrease conductivity by generating a soft gap. Here we approach the problem from the opposite side of the phase diagram. Starting with a correlated insulator we demonstrate experimentally that a chemical disorder can also induce a power-law gap which does not require any additional order parameter for its existence.

Materials and Methods

Sr327 single crystals used in our experiments were grown by the conventional flux methods[33], cleaved at ~77 K in ultra-high vacuum and immediately inserted into the STM head where they are held at ~5 K during the process of data acquisition. All dI/dV measurements were taken using a standard lock-in technique with ~5-10mV peak to peak modulation. Tungsten tips were annealed and then prepared on Cu single crystal surface before using on iridate samples.

X-ray absorption spectroscopy measurements were performed using the Soft X-ray Microcharacterization Beamline (SXRMB) at the Canadian Light Source. Measurements were carried out at the Ru L3 ($2p_{3/2}$ to 4d) and L2 ($2p_{1/2}$ to 4d) absorption edges, which occur at energies of 2838 eV and 2967 eV respectively. Data were collected using both Total Electron Yield (TEY) and Fluorescence Yield (FY) detection modes. Energy calibration was verified by a comparison of Ar K edge features observed at E = 3206 eV. In order to improve counting statistics and verify the reproducibility of the data, multiple scans were performed on each sample. Each dataset shown in Fig. 1C or Fig. S2 consists of three or more individual scans which have been binned together. Each scan has been normalized such that the edge jump associated with the Ru absorption edge has been set to unity.

Acknowledgements

V.M. gratefully acknowledges funding from NSF Award No. DMR-1610143 for the STM studies. The theoretical collaboration was supported by DMREF 1629382 and NSF DMREF 1629068 and in part by the Gordon and Betty Moore Foundation's EPiQS Initiative through the Grant No. GBMF4305 at the Institute for Condensed Matter Theory of the University of Illinois (L. S). S.D.W. acknowledges funding support from NSF Award No. DMR-1505549. Research at the University of Toronto was supported by the NSERC, CFI, OMRI, and Canada Research Chair program. We used the Canadian Light Source, which is funded by the Canada Foundation for Innovation, the Natural Sciences and Engineering Research Council of Canada, the National Research Council Canada, the Canadian Institutes of Health Research, the Government of Saskatchewan, Western Economic Diversification Canada, and the University of Saskatchewan.

1. Imada M, Fujimori A, Tokura Y (1998) Metal-insulator transition. *Rev Mod Phys* 70: 1039
2. Dagotto Elbio (2005) Complexity in strongly correlated electronic systems. *Science* 309: 257-262
3. Richardella A *et al* (2010) Visualizing critical correlations near the Metal-Insulator transition in $Ga_{1-x}Mn_xAs$. *Science* 327: 665-669
4. Anderson P W (1958) Absence of diffusion in certain random lattices. *Phys Rev* 109: 1492
5. Mott NF (1949) The basis of the electron theory of metals, with special reference to the transition metals. *Proc Phys Soc* Sect A 62: 416
6. Alloul H, Bobroff J, Gabay M, Hirschfeld PJ (2009) Defects in correlated metals and superconductors. *Rev Mod Phys* 81: 45-108
7. Lee PA, Nagaosa N, Wen X-G (2006) Doping a Mott insulator: Physics of high-temperature superconductivity. *Rev Mod Phys* 78: 17-84
8. Altshuler BL, Aronov AG (1979) Zero bias anomaly in tunnel resistance and electron-electron interaction. *Solid State Commun* 30: 115
9. Efros AL, Shklovskii BI (1975) Coulomb gap and low temperature conductivity of disordered systems. *J Phys C* 8: L49
10. Butko VY, DiTusa Jf, Adams PW (2000) Coulomb gap: How a metal film becomes an insulator. *Phys Rev Lett* 84: 1543
11. Heidarian D, Trivedi N (2004) Inhomogeneous metallic phase in a disordered Mott Insulator in two dimensions. *Phys Rev Lett* 93: 126401
12. Fazileh F, Gooding RJ, Atkinson WA, Johnston DC (2006) Role of strong electronic correlations in the metal-to-insulator transition in disordered $LiAl_yTi_{2-y}O_4$. *Phys Rev Lett* 96**:** 046410
13. Chiesa S *et al* (2008) Disorder-induced stabilization of the pseudogap in the strongly correlated system. *Phys Rev Lett* 101: 086401
14. Shinaoka H, Imada M (2009) Soft Hubbard gaps in disordered itinerant models with short-range interaction. *Phys Rev Lett* 102, 016404
15. Chen H-Y *et al* (2011) Disorder-induced zero-bias anomaly in the Anderson-Hubbard model: Numerical and analytical calculations. *Phys Rev B* 84: 045113
16. Dobrosavljevic V, Kotliar G (1997) Mean Field Theory of the Mott-Anderson Transition. *Phys Rev Lett* 78: 3943
17. Byczuk K, Hofstetter W, Vollhardt D (2005) Mott-Hubbard Transition versus Anderson Localization in Correlated Electron Systems with Disorder. *Phys Rev Lett* 94: 056404
18. Aguiar MCO, Dobrosavljevic V (2013) Universal quantum criticality at the Mott-Anderson transition. *Phys Rev Lett* 110: 066401
19. Hanaguri T *et al* (2004) A 'checkerboard' electronic crystal state in lightly hole-doped $Ca_{2-x}Na_xCuO_2Cl_2$. *Nature* 430: 1001-1005
20. Kohsaka Y *et al* (2007) An intrinsic bond-centered electronic glass with unidirectional domains in underdoped cuprates. *Science* 315: 1380-1385
21. Kohsaka Y *et al* (2012) Visualization of the emergence of the pseudogap state and the evolution to superconductivity in a lightly hole-doped Mott insulator. *Nature Phys* 8: 534
22. Cai P *et al* (2016) Visualizing the evolution from the Mott insulator to a charge-ordered insulator in lightly doped cuprates. *Nature Phys* 12: 1047-1051
23. Battisti I *et al* (2017) Universality of pseudogap and emergent order in lightly doped Mott insulator. *Nature Phys* 13, 21-25
24. Yan YJ *et al* (2015) Electron-doped Sr_2IrO_4: An analogue of hole-doped cuprate superconductors demonstrated by Scanning Tunneling Microscopy. *Phys Rev X* 5: 041018
25. Qiao S *et al* (2017) Mottness collapse in 1T-$TaS_{2-x}Se_x$ transition-metal dichalcogenide: An interplay between localized and itinerant orbitals. *Phys Rev X* 7: 041054
26. Cun Y *et al* (2015) Strong similarities between the local electronic structure of insulating iron pnictides and lightly doped cuprate. *Phys Rev X* 5: 021013
27. Song Y *et al* (2016). A Mott insulator continuously connected to iron pnictides superconductors. *Nature Comm* 7: 13879
28. Kim BJ *et al* (2008) Novel $J_{eff}=1/2$ Mott state induced by relativistic spin-orbit coupling in Sr_2IrO_4. *Phys. Rev. Lett.* 101: 076402
29. Moon SJ *et al* (2008) Dimensionally-controlled insulator-metal transition and correlated metallic state in 5d transition metal oxides $Sr_{n+1}Ir_nO_{3n+1}$(n=1,2, and ∞). *Phys Rev Lett* 101: 226402
30. Kim YK *et al* (2014) Fermi arcs in a doped pseudospin-1/2 Heisenberg antiferromagnet. *Science* 345: 187
31. Kim YK *et al* (2016) Observation of a d-wave gap in electron-doped Sr_2IrO_4. *Nat Phys* 12: 37-41
32. Okada Y *et al* (2013). Image the evolution of metallic states in a correlated iridate. *Nat Mater* 12: 707–713
33. Dhital C *et al* (2014) Carrier localization and electronic phase separation in a doped spin-orbit-driven Mott phase in $Sr_3(Ir_{1-x}Ru_x)_2O_7$. *Nature Comm* 5: 3377
34. Li L *et al* (2013) Tuning the $J_{eff}=1/2$ insulating state via electron doping and pressure in the double-layered iridate $Sr_3Ir_2O_7$. *Phys Rev B* 87: 235127
35. Cao Y *et al* (2016) Hallmarks of the Mott-metal crossover in the hole-doped pseudospin-1/2 Mott insulator Sr_2IrO_4. *Nature Comm* 7: 11367
36. Wadati H *et al* (2010) Where are the extra d electrons in transition-metal-substituted iron pnictides? *Phys Rev Lett* 105: 157004
37. Levy G *et al* (2012) Probing the role of Co substitution in the electronic structure of iron pnictides. *Phys Rev Lett* 109: 077001
38. Clancy JP *et al* (2014) Dilute magnetism and spin-orbital percolation effects in $Sr_2Ir_{1-x}Rh_xO_4$. *Phys Rev B* 89: 054409
39. Calder S *et al* (2015) Evolution of competing magnetic order in the J=1/2 insulating state of $Sr_2Ir_{1-x}Ru_xO_4$. *Phys Rev B* 92: 165128
40. Cao Y *et al* (2017) Giant spin gap and magnon localization in the disordered Heisenberg antiferromagnet $Sr_2Ir_{1-x}Ru_xO_4$. *Phys Rev B* 95: 121103(R)
41. Iwaya K *et al* (2007) Local tunneling spectroscopy across a metamagnetic critical point in the bilayer ruthenate $Sr_3Ru_2O_7$. *Phys Rev Lett* 99: 057208
42. Shante VK, Kirkpatrick S (1971) An introduction to percolation theory. *Adv Phys* 20: 325-357
43. Lahoud E *et al* (2014) Emergence of a novel pseudogap metallic state in a disordered 2D Mott insulator. *Phys Rev Lett* 112: 206402
44. Shinaoka H *et al* (2009) Single-particle excitations under coexisting electron correlation and disorder: a numerical study of the Anderson-Hubbard model. *J Phys Soc Jpn* 78: 094708
45. Kim J *et al* (2006) Photoemission and X-ray absorption study of the electronic structure of $SrRu_{1-x}Ti_xO_3$. *Phys Rev B* 73: 235109
46. Pan Z-H *et al* (2009) Evolution of Fermi Surface and normal-state gap in the chemically substituted cuprate $Bi_2Sr_{2-x}Bi_xCuO_{6+\sigma}$. *Phys Rev B* **79**: 092507
47. Tanaka K *et al* (2006) Distinct Fermi-momentum- dependent energy gaps in deeply underdoped Bi2212. *Science* 314: 1910
48. Mannella N *et al* (2005) Nodal quasiparticle in pseudogapped colossal magnetoresistive manganites. *Nature* 438: 474-478

Figure 1. Insulator-metal transition in $Sr_3(Ir_{1-x}Ru_x)_2O_7$. (A) Phase diagram of $Sr_3(Ir_{1-x}Ru_x)_2O_7$ established by bulk susceptibility, neutron scattering and transport measurements in ref. 33. CAF-I: insulating canted AF phase; PM-I: paramagnetic insulating phase; AF-M: AF ordered metallic phase; PM-M: paramagnetic metal. (B) Temperature-dependent resistivity for different Ru concentrations. IMT takes place at the critical concentration of x∼0.37. (C) Comparison of the Ru oxidation state in $Sr_3(Ir_{1-x}Ru_x)_2O_7$ with other reference samples using X-ray absorption spectroscopy. The oxidation states of Ru in $RuCl_2$, RuI_3, $RuCl_3$ and RuO_4 are 2+, 3+, 3+ and 4+ respectively. (D) Topography taken on 50% Ru-doped samples. Scanning conditions: V_b=200mV, I=50pA. V_b: sample bias with respect to the tip; I: set point current.

Figure 2. *dI/dV* line cuts across IMT in $Sr_3(Ir_{1-x}Ru_x)_2O_7$. Line cuts and the associated topographic images indicating where the line cuts were obtained in: (A) 27%, (B) 35%, and (C) 50% Ru-substituted samples. The spectra in A and B show the evolution from gapped and insulating line-shape (27%), to relatively smaller gap and more metallic behavior (35%). The spectra of 50% Ru-doped sample shown in C, however, exhibit V-shaped DOS almost along the whole line. STM setup condition in all panels: V_b=-200mV, I=100pA. The spectra have been shifted vertically for clarity.

Figure 3. Spatial evolution of *dI/dV* spectra for a wide range of Ru substitution. (A-C) Gap maps showing the spatial inhomogeneity. The metallic regions expand (red) as the Ru concentration increases, indicating the trend towards an IMT. (D) *dI/dV* conductance map at +30mV for x=0.5 Ru- substituted sample. (E-G) Averaged *dI/dV* spectra for x∼27%, x∼35% and x∼38%, respectively. To create these averages, spectra in the dI/dV maps were sorted by the gap magnitude into bins and then each bin was averaged. The spectra were split into ∼20 bins with equal population, ranging from the ones with the largest gap (blue/purple) to the ones with zero gap (red). The colors for the spectra at each doping depict the spectra in the same color regions of the gap maps at that doping. (H) Averaged spectra which are classified by the conductance value at +30mV. At this Ru concentration, all spectra are gapless. The color scale indicates the conductance value (see section VIII). (I) Histograms of the spectral gap magnitude. The average gap size shrinks as the Ru substitution increases.

Figure 4. Characterizing the V-shape gap. (A) Fit to the most metallic dI/dV spectra shown in Fig. 3 for x=0.27, 0.35 and 0.38 , and the most V- shaped one in Ru=0.5, with $a|(E-E_F)|^p$. The spectra have been shifted vertically for clarity, and the dashed lines denote the position of zero conductance for each curves. (B) Range of fitting parameter *p* for the data shown in Fig. 3E-H. The index numbers label the bins described in Fig. 3. A smaller power corresponds to a more metallic spectrum.